NATURALISTA CAMPANO
ISSN: 1827-7160
Volume 28 Issue 1, 2024

Rail Anomaly Recognition Method Using Haralick Features and AFNN Detector

Yang Liyuan[1,2*], Ghazali Osman[2]

[1,2]College of Computing, Informatics and Mathematics, Universiti Teknologi MARA, Malaysia.
[2]College of Computing, Informatics and Mathematics, Kunming University, Kunming, Yunnan, China.

Email: 1335647006@qq.com

Abstract: Rail abnormalities can lead to traffic accidents causing personal and property losses, making timely detection of these anomalies crucial for rail transportation. However, the current discovery of rail abnormalities relies mainly on subjective human observation, lacking mature machine vision-based detection methods. This study proposes a new AFNN detector based on the extraction of Haralick features and the development of a fuzzy neural network for identifying rail abnormalities. Experimental results demonstrate that this method achieves rail abnormality recognition, with the identification performance of Haralick features surpassing that of colour features and HU features, achieving an accuracy of 0.9186.

Keywords: Haralick Features, Fuzzy Detector, Rail Anomaly.

1. Introduction

Steel rails constitute a vital component of railway infrastructure (Figure 1). Their primary function is to guide the wheels of locomotives and rolling stock, bearing immense pressure while transmitting it to the sleepers. Steel rails are required to furnish a continuous, smooth, and minimally resistant rolling surface for the wheels. In electrified railways or sections with automatic block signalling, rails also serve as conductors for track circuits, facilitating the return flow of traction currents.

Figure 1: Wheels and rails

As a pivotal component of rail transportation, rails bear direct loads from heavy vehicles and encounter impacts and friction from wheelsets. Moreover, being exposed to outdoor conditions, such as sunlight, rain corrosion, steel oxidation, and various forces, rail surfaces manifest diverse forms of anomalies. These irregular, multifarious, and multi-scaled anomalies pose significant challenges (Figure 2). In operational maintenance, failure to promptly detect these damages can lead to severe safety hazards. The occurrence of accidents could result in incalculable human casualties and property loss. Hence, timely detection of rail anomalies is paramount for mitigating risks and ensuring the safe operation of railways before catastrophic incidents occur.

Normal	Abnormal			
	Scratch	Block	Chap	Scab

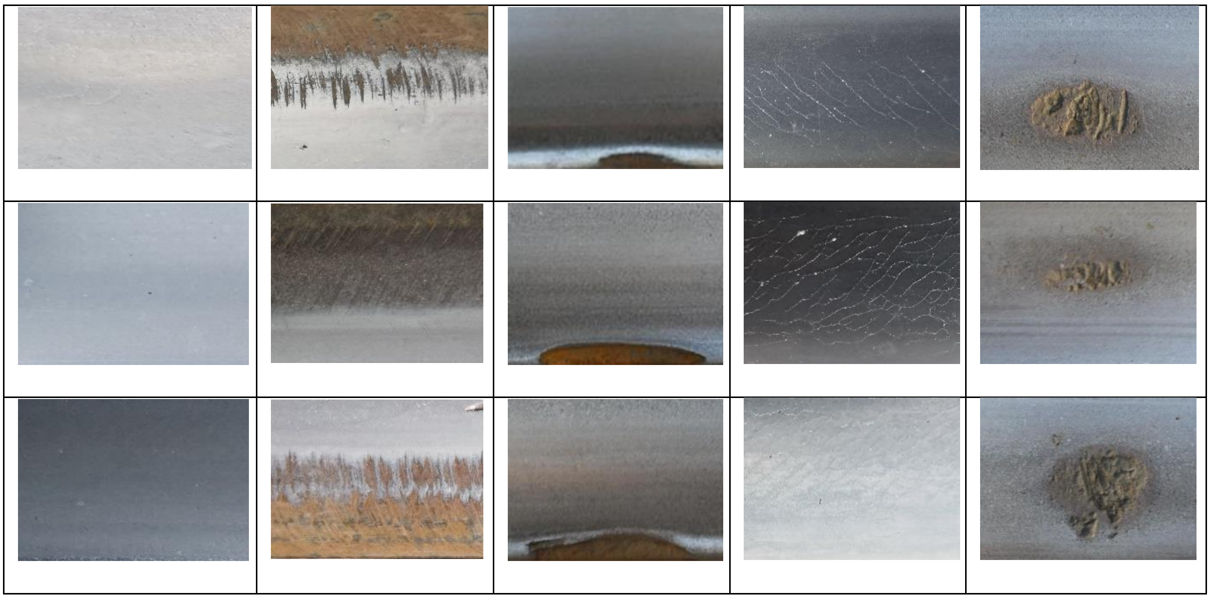

Figure 2: Normal rail and abnormal rail

2. Literature Review

Min et al. (2018) introduced a real-time detection system for rail surface defects utilizing machine vision. By employing the H component of the hue, saturation, and lightness (HSL) space as a feature, rail regions were extracted from panoramic images, followed by surface defect segmentation using image morphological operations. Subsequently, algorithms were validated through the construction of a prototype detection system. He et al. (2014, 2016) proposed rail surface defect detection systems based on reverse Perona-Malik (P-M) diffusion and background difference techniques. Li and Ren (2012a, 2012b) focused on visual characteristics of defect targets, designing contrast enhancement algorithms suitable for rail defect detection. They introduced defect localization algorithms based on projection contours and defect detection algorithms utilizing proportionally enhanced maximum entropy. Zhang et al. (2018) utilized curvature filtering and an improved Gaussian mixture model to detect rail surface defects, enhancing identification precision through region of interest (ROI) detection extraction algorithms, grayscale contrast algorithms, and curvature filtering. Min et al. (2018) proposed a method based on image grayscale gradient features for rail surface defect detection, effective in identifying scars and crack defects while mitigating external environmental interference in machine vision detection of rail surfaces. Additionally, Karakose et al. (2018, 2017) developed computer vision-based techniques for condition monitoring and fault diagnosis of rail components and tracks, utilizing camera installations on simulated train bottoms and tops. Their approach involved Canny edge detection and Hough transform methods for target detection, followed by decision tree classification for identifying track types and classifying surface anomalies.

Despite meeting real-time detection requirements, these methods exhibit high false alarm rates and challenges in accurately identifying anomalous targets. This study endeavours to address these issues by extracting Haralick features and employing a novel AFNN detector based on fuzzy neural networks, thus offering a fresh perspective for rail anomaly detection research.

3. Methodology

3.1 Dataset and Preprocessing

In the realm of railway engineering, datasets focusing on the classification and detection of railway defects have garnered attention (Zendel et al., 2019). However, the availability of authentic datasets specifically tailored for railway surface defects remains limited. Gathering data on rail surface anomalies poses challenges due to their random distribution and operational constraints in high-speed railway management. The NEU dataset (Song et al., 2013) primarily addresses surface defect issues in hot-rolled steel strips, encompassing anomalies such as patches, cracks, and scratches. Although comprising 1800 images and sharing the same material as rails, it fails to comprehensively represent rail surface anomalies. The Rail-5k dataset, compiled by Zhang et al. (2021) consists of 5000 images of railway defects, aiming to identify the most common 13 types of defects. Regrettably, these datasets remain unpublished for public use. Hence, there is an urgent need to develop more suitable datasets for rail anomaly research. To obtain the dataset for this study, we captured 427 images on-site from various locations in Yunnan Province, China. These images were divided into training and validation sets in a ratio of 0.8:0.2. The collected data underwent the following preprocessing steps:

1. Cropping images to a size of 448x448 pixels cantered on the anomalous regions.
2. Converting colour images to grayscale.
3. Performing histogram equalization.
4. Employing Gaussian filtering for noise reduction.

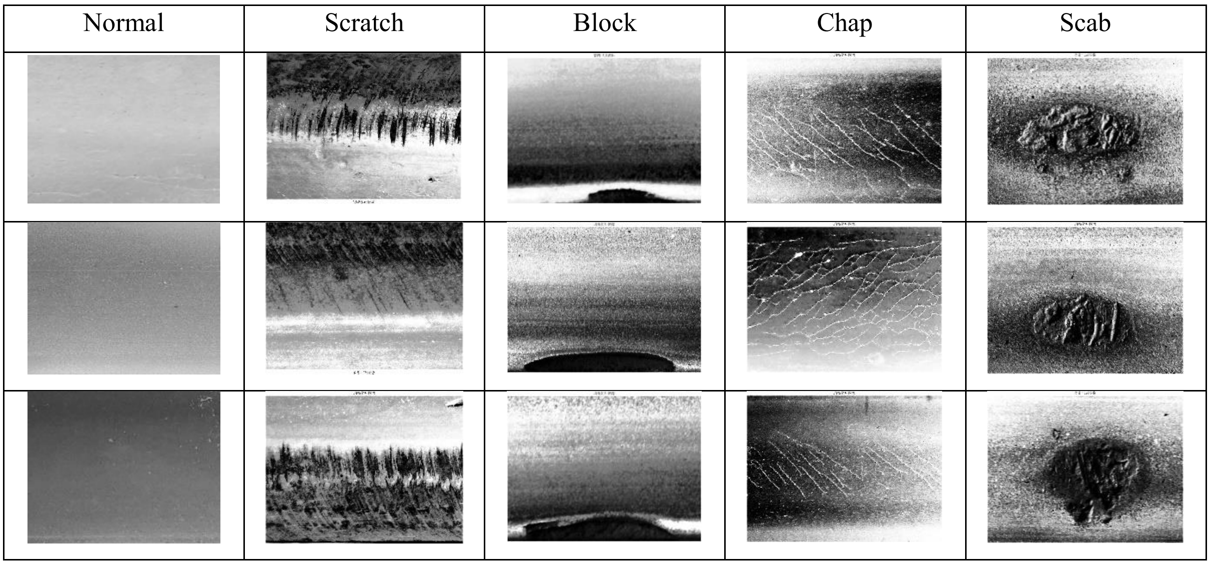

Figure 3 display the grayscale images of rails post-processing.

3.2 Feature Extraction

A pivotal aspect of classification recognition lies in feature extraction, a methodological process where computers extract characteristic information from images. The primary objective is to obtain relevant information from the low-dimensional spatial information representation of raw data. In this study, Haralick Features were utilized for anomaly recognition. Haralick features, widely employed in texture analysis, are instrumental in image processing and computer vision. These features describe texture characteristics within images and aid in identifying texture disparities among different regions. Consequently, they find extensive application in various image classification, segmentation, and recognition tasks. Calculation of Haralick features relies on the Gray Level Co-occurrence Matrix (GLCM), a statistical matrix describing image texture. The GLCM signifies the relative positional relationships between different pixel values in an image, constructed by tallying the co-occurrence frequencies of grayscale levels of each pixel with its neighboring pixels. It reflects comprehensive information about grayscale variations concerning direction, adjacent spacing, and intensity changes, analyzing local patterns and their arrangement rules. In essence, the GLCM computes the probability of a pixel with a grayscale value i at distance (dx, dy) from another pixel having a grayscale value j. Formula 1 is the mathematical expression for the GLCM, where d represents the relative distance in terms of pixel counts, θ denotes the direction (typically chosen as four directions: 0°, 45°, 90°, and 135°), and (x, y) represent the pixel coordinates within the image.

$$P(i,j|d,\theta) = \{(x,y)|f(x,y)=i, f(x+dx,y+dy)=j; x,y=0,1,2,\ldots,N-1\} \quad (1)$$

As illustrated in Figure 4, the x-direction corresponds to the columns of the image, while the y-direction corresponds to the rows. F(x, y) = i represents the pixel value at coordinates (x, y), and the count (normalized: probability) of occurrences where f(x + dx, y + Dy) = j at a distance (dx, Dy) needs to be statistically recorded. The selection of (dx, Dy) induces variations in the angle, typically chosen as 0°, 45°, 90°, and 135°.

NATURALISTA CAMPANO
ISSN: 1827-7160
Volume 28 Issue 1, 2024

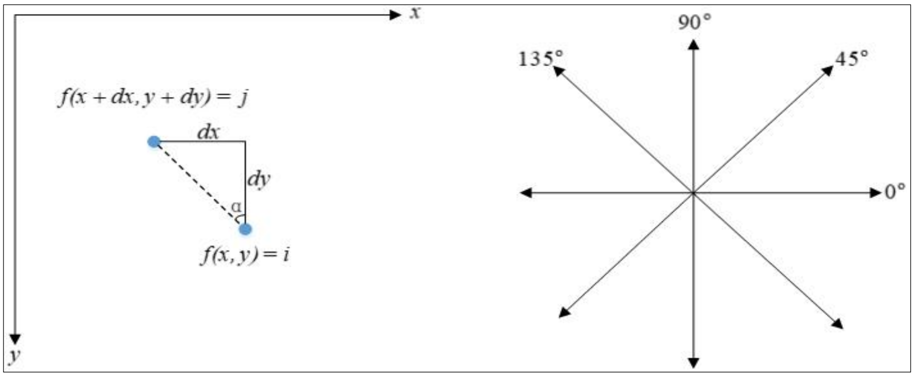

Figure 4: Statistical direction of pixel value i

The constructed co-occurrence matrix serves as the basis for extracting texture features. In this study, the texture features of images were computed using 13 parameters of Haralick features. These 13 feature parameters of Haralick features include Energy (Energ), Variance (Sosvh), Contrast (Contr), Correlation (Corrm), Homogeneity (Homom), Sum average (Savgh), Sum variance (Svarh), Sum entropy (Senth), Entropy (Entro), Difference variance (Dvarh), Difference entropy (Denth), Information measure of correlation1 (Inf1h), and Information measure of correlation2 (Inf2h). Table 1 elucidates the physical interpretations and computational formulas associated with these 13 parameters of Haralick features.

Table 1: Physical meanings and computation formulas of parameters of Haralick features.

Parameters	Physical Meaning	Formula
Energ	Measures the uniformity and regularity of image texture	$Energ = \sum_i \sum_j p(i,j)^2$ (2)
Sosvh	Characterizes irregularities and variations in image texture	$Sosvh = \sum_i \sum_j (i-\mu)^2 p(i,j)$ (3)
Contr	Assesses the degree of contrast between different grayscale levels in the image	$Contr = n^2 \left\{\sum_{i=1}^{Ng} \sum_{j=1}^{Ng} p(i,j)\right\} \lvert i-j \rvert = n$ (4)
Corrm	Quantifies the correlation between GLCM elements, reflecting the linear characteristics of image texture	$Corrm = \frac{\sum_i \sum_j (ij)p(i,j) - \mu_x \mu_y}{\sigma_x \sigma_y}$ (5)
Homom	Signifies the degree of consistency among texture elements in the image	$Homom = \sum_i \sum_j \frac{1}{1+(i-j)^2} p(i,j)$ (6)
Savgh	Reflects the average distribution of texture elements with the same grayscale level in the image	$Savgh = \sum_{i=2}^{2Ng} i p_{x+y}(i,j)$ (7)
Svarh	Measures the distribution variance of texture elements with the same grayscale level	$S\,\text{var}\,h = \sum_{i=2}^{2Ng} (i-f_S)^2 p_{x+y}(i)$ (8)
Senth	Represents the distribution entropy of texture elements in the image, indicating the uncertainty of their distribution	$Senth = -\sum_{i=2}^{2Ng} p_{x+y}(i) \log\{p_{x+y}(i)\} = f_S$ (9)
Entro	Measures the overall entropy of GLCM elements, representing the overall uncertainty of image texture	$Entro : -\sum_i \sum_j p(i,j) \log(p(i,j))$ (10)
Dvarh	Reflects the variance of differences between different grayscale levels in the image	$D\,\text{var}\,h = \sum_{i=0}^{Ng-1} i^2 p_{x-y}(i)$ (11)
Denth	Reflects the variance of differences between different grayscale levels in the image, indicating the uncertainty of differences	$Denth = -\sum_{i=0}^{Ng-1} p_{x-y}(i) \log\{p_{x-y}(i)\}$ (12)
Inf1h	Related to correlation but incorporates the concept of entropy in its calculation, providing a more comprehensive description of the correlation and uncertainty of image texture	$Inf1h = \frac{HXY - HXY1}{\max\{HX, HY\}}$ (13)

Inf2h	Related to correlation but employs different mathematical formulas to provide a more precise description of the correlation and uncertainty of image texture	$Inf2h = (1-\exp[-2[HXY2-HXY]])^{\frac{1}{2}}$ (14)

3.3 AFNN Detector

The Adaptive Fuzzy Neural Network (AFNN) possesses learning and self-adjusting capabilities, continuously enhancing network performance, thereby well-suited to address the complexities encountered in rail anomaly detection. Consequently, leveraging the extracted low-order feature data, this study constructed a Fuzzy Anomaly Detector (AFNN) utilizing a combination of Forward Neural Network (FNN) and Adaptive Neuro-Fuzzy Inference System (ANFIS) implemented within the PyTorch framework. During the training phase, AFNN employed a cross-entropy loss function and adjusted learning rates using a learning rate scheduler. In the testing phase, the model computed and outputted accuracy metrics on the test set, saving model weights based on a predefined accuracy threshold (0.85). Additionally, the model defined a confusion matrix function to visualize classification results on the test set.

The AFNN classifier comprises five linear layers, namely the fuzzy membership function layer, fuzzy rule layer, fuzzy inference layer, input layer, and output layer. By amalgamating the fuzzy membership function layer, fuzzy rule layer, and fuzzy inference layer, the AFNN introduces fuzzy logic principles to model the intricate relationships between inputs and outputs. Model parameters are initialized using a uniform distribution, with Tanh serving as the activation function. The extracted Haralick Features are inputted into the AFNN classifier for rail anomaly classification. Figure 5 illustrates the forward propagation process and network structure of the AFNN classifier.

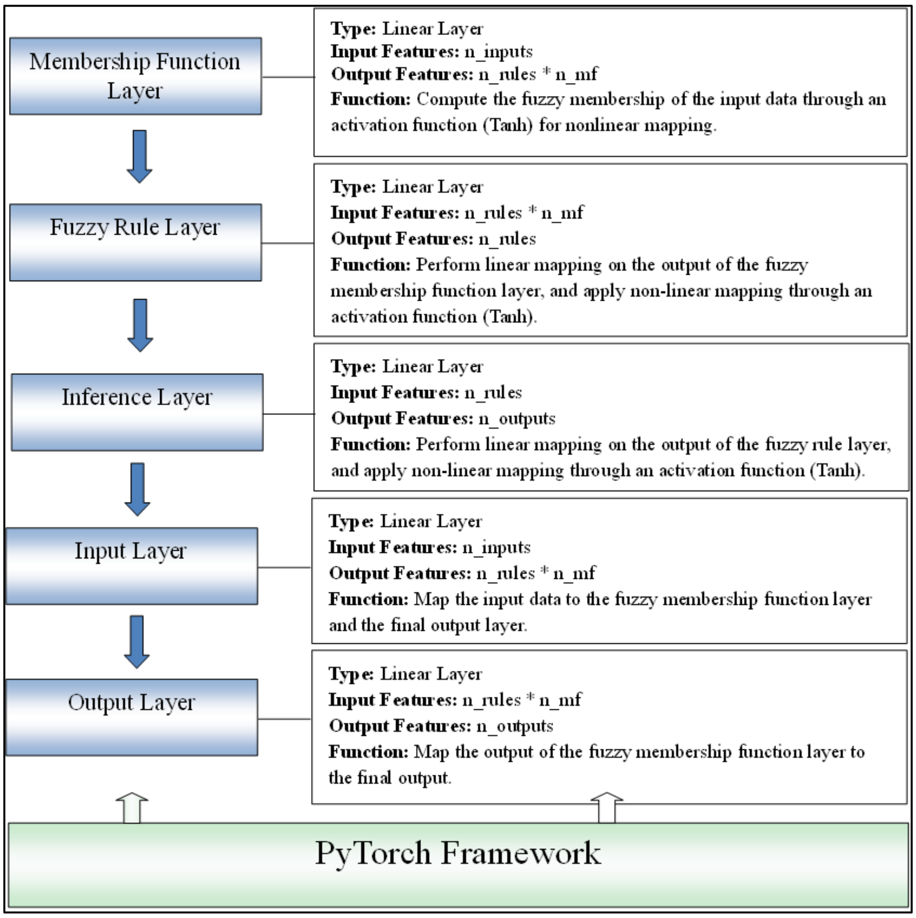

Figure 5: Network structure of AFNN

This sequence of operations ensures that the model learns the complex relationship between inputs and outputs through the combination of fuzzy membership functions, fuzzy rules, and fuzzy inference. Throughout the entire process, linear mappings are achieved through the Linear layer, while non-linear mappings are facilitated by the Tanh activation function. The Tanh activation function (hyperbolic tangent function) stands as a commonly utilized non-linear activation function, typically employed within neural network hidden layers. It compresses input values into the interval [-1, 1] and exhibits an S-shaped curve. Formula 15 illustrates the definition of the Tanh activation function, where e represents the base of the natural logarithm and x denotes the input value.

$$Tanh(x) = \frac{e^x - e^{-x}}{e^x + e^{-x}} \tag{15}$$

The Cross-Entropy Loss function, utilized in this study, serves as a metric for assessing the disparity between the probability distributions of predicted values and actual labels. Notably, it possesses characteristics of simple gradient computation, rapid gradient descent, and insensitivity to outliers. Herein, the Cross-Entropy Loss is defined as the loss function. Formula 16 delineates the calculation formula for the Cross-Entropy Loss, where N represents the number of samples, $y_{i,k}$ denotes the true label of the k-th category for the i-th sample, and $p_{i,k}$ signifies the predicted probability of the k-th category for the i-th sample.

$$loss = -\frac{1}{N}\sum_{i=1}^{N}\sum_{k=1}^{K} y_{i,k}\, log\left(p_{i,k}\right) \tag{16}$$

In summary, the AFNN classifier represents an adaptive fuzzy classifier based on Haralick features. A distinctive feature of this classifier is the incorporation of fuzzy logic into neural networks, achieved through the amalgamation of fuzzy membership function layer, fuzzy rule layer, and fuzzy inference layer. This integration enables the model to effectively handle fuzzy information and uncertainty. Moreover, the model exhibits adaptability, capable of learning the fuzzy characteristics and intricate rules of input data, culminating in the final output through fuzzy inference.

3.4 Results evaluation

The recognition outcomes are evaluated using Precision, Recall, and Accuracy based on True Positive (TP), False Positive (FP), True Negative (TN), and False Negative (FN). Herein, TP represents the number of anomalous rails correctly identified as anomalies by the model; FP denotes the number of normal rails erroneously classified as anomalies by the model; TN signifies the number of normal rails incorrectly classified as anomalies by the model; while FN indicates the number of anomalous rails erroneously classified as normal by the model.

Precision: Precision refers to the proportion of truly anomalous samples among those predicted as rail anomalies by the model. It measures the accuracy of the model in predicting anomalies. Higher precision signifies greater reliability in anomaly detection. Formula 17 illustrates the calculation method for Precision.

$$Pr\,e\,cision = \frac{TP}{TP+FP} \tag{17}$$

Recall: The recall rate refers to the proportion of all actual rail abnormal samples that the model successfully predicts as abnormal. The recall rate is also called True Positive Rate. Calculation 18 shows the calculation method of Recall.

$$Re\,c\,all = \frac{TP}{TP+FN} \tag{18}$$

Accuracy: Accuracy refers to the ratio of the number of samples correctly predicted by the model to the total number of samples. It measures the overall correctness of the model across all categories. Equation 19 shows how Accuracy is calculated.

$$Accuracy = \frac{TP+TN}{TP+TN+FP+FN} \tag{19}$$

The evaluation metrics are crucial tools for assessing the results, providing quantifiable measures of the experimental methods' performance. This study comprehensively investigates the recognition performance of Haralick feather in identifying rail anomalies under different color models, by considering accuracy, recall, and precision.

4. Results and Discussion

The experiment utilized 427 preprocessed images of rail anomalies, comprising 200 normal instances, 56 scratches, 60 blocks, 56 chaps, and 55 scabs. Following the extraction of Haralick Features, the images were inputted into the developed AFNN classifier for anomaly recognition. The evaluation of results employed metrics such as True

Positive (TP), True Negative (TN), False Positive (FP), False Negative (FN), and confusion matrices. Additionally, the study conducted comparative analyses with HU features and color features extracted from color images. Tables 2-4 present the rail anomaly recognition results obtained using Haralick Features, color features, and HU features. Furthermore, Figure * depicts the confusion matrices illustrating these results.

Table 2: Recognition results utilizing Haralick Features.

Type	Normal	Scratch	Block	Chap	Scab
TP	39	13	11	8	8
FP	3	0	1	1	2
TN	44	390	72	145	74
FN	0	1	2	2	2
Precision	0.9286	1.0000	0.9167	0.8889	0.8000
Recall	1.0000	0.9286	0.8462	0.8000	0.8000
Accuracy	0.9651	0.9975	0.9651	0.9808	0.9535
AVG-accuracy	0.9186				

Table 3： Recognition results utilizing Color Features.

Type	Normal	Scratch	Block	Chap	Scab
TP	35	10	15	9	5
FP	2	3	1	3	5
TN	45	365	68	121	73
FN	4	0	2	5	3
Precision	0.9459	0.7692	0.9375	0.7500	0.5000
Recall	0.8974	1.0000	0.8824	0.6429	0.6250
Accuracy	0.9302	0.9921	0.9651	0.9420	0.9070
AVG-accuracy	0.8605				

Table 4： Recognition results utilizing HU Features.

Type	Normal	Scratch	Block	Chap	Scab
TP	44	6	12	8	11
FP	45	2	3	1	7
TN	28	419	72	167	68
FN	2	11	7	13	1
Precision	0.4944	0.7500	0.8000	0.8889	0.6111

Recall	0.9565	0.3529	0.6316	0.3810	0.9167
Accuracy	0.6050	0.9703	0.8936	0.9259	0.9080
AVG-accuracy	0.6512				

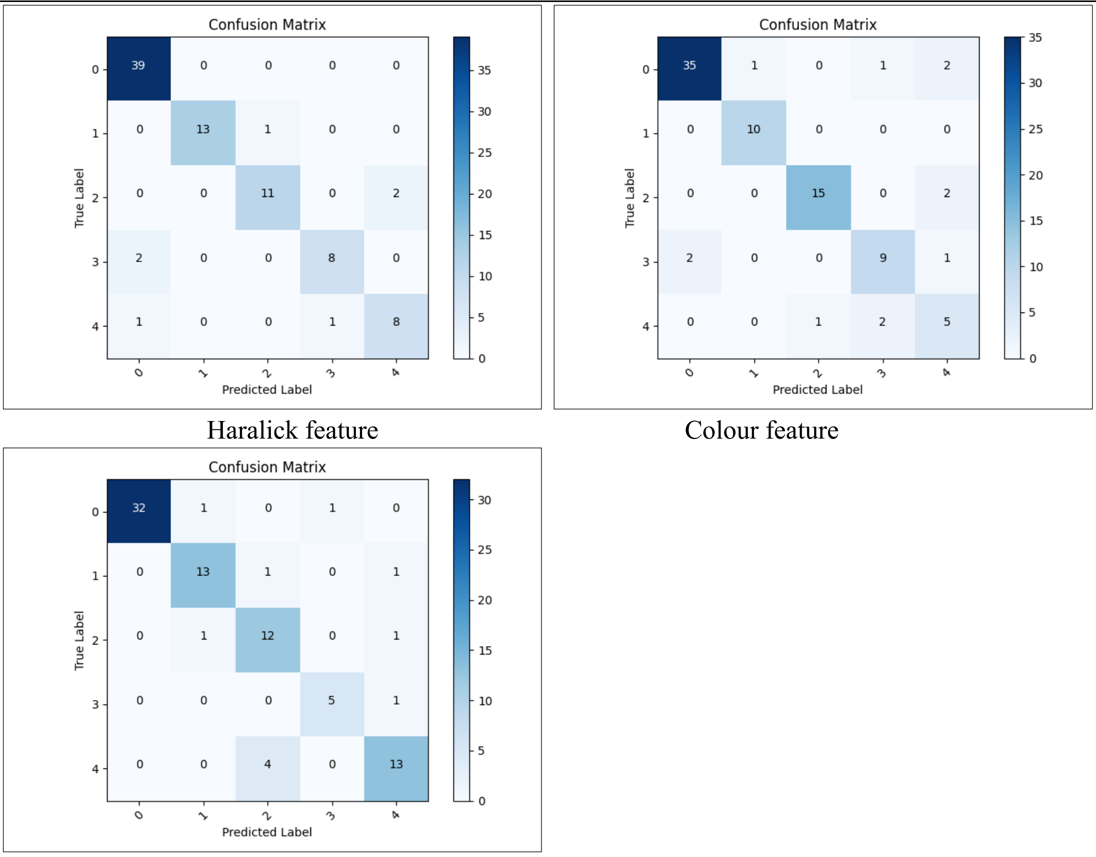

Haralick feature

Colour feature

HU feature

Figure 6: Confusion matrix of validation set

From the figures and tables, it is evident that the AFNN detector exhibits commendable performance in rail anomaly recognition, demonstrating proficiency in identifying various types of rail anomalies. Notably, Haralick Features outperform the other two types of features, achieving a superior performance in rail anomaly recognition with a multi-classification recognition accuracy of 0.9186. Specifically, the recognition accuracies for the five rail anomaly categories, namely Normal, Scratch, Block, Chap, and Scab, reached 0.9651, 0.9975, 0.9651, 0.9808, and 0.9535, respectively.

5. Conclusion

In exploring effective features for rail anomaly recognition, this study employed Haralick Features and a newly developed AFNN detector based on model neural networks for multi-classification recognition of rail anomalies. Experimental results indicate the commendable detection efficacy of the AFNN detector in rail anomaly detection, with Haralick Features exhibiting superior recognition performance compared to color features and HU features, achieving an overall accuracy of 0.9186.

6. Reference

1. He Z., D., Wang Y. N., Mo J. X, & Yin F. (2014). Visual detection of rail surface defects based on reverse PM diffusion. Acta Automatica Sinica, 40(8), 1667-1679.

2. He Z. D., Wang Y. N., Liu J., & Yin F. (2016). High-speed rail surface defect image segmentation based on background difference. Journal of Instrumentation, 37(3), 640-649.
3. Karakose, M., Yaman, O., Murat, K., & Akin, E. (2018). A new approach for condition monitoring and detection of rail components and rail track in railway. International Journal of Computational Intelligence Systems, 11(1), 830-845.
4. Karakose, M., Yaman, O., Baygin, M., Murat, K., & Akin, E. (2017). A new computer vision based method for rail track detection and fault diagnosis in railways. International Journal of Mechanical Engineering and Robotics Research, 6(1), 22-17.
5. Li, Q., & Ren, S. (2012). A real-time visual inspection system for discrete surface defects of rail heads. IEEE Transactions on Instrumentation and Measurement, 61(8), 2189-2199.
6. Melissa T. Baysari and Andrew S. McIntosh and John R. Wilson. (2008). Understanding the human factors contribution to railway accidents and incidents in Australia. Accident Analysis and Prevention, 40(5), pp. 1750-1757.
7. Min, Y., Xiao, B., Dang, J., Yue, B., & Cheng, T. (2018). Real time detection system for rail surface defects based on machine vision. EURASIP Journal on Image and Video Processing, 2018(1), 1-11.
8. Song, K., & Yan, Y. (2013). A noise robust method based on completed local binary patterns for hot-rolled steel strip surface defects. Applied Surface Science, 285, 858-864.
9. Zhang H., Jin X. T., Jonathan, W. Q., He Z. D., & Wang Y. N. (2018). Automatic visual detection method of rail defects based on curvature filtering and improved GMM. Journal of Instrumentation, 39(4), 181-194.
10. Zendel, O., Murschitz, M., Zeilinger, M., Steininger, D., Abbasi, S., & Beleznai, C. (2019). Railsem19: A dataset for semantic rail scene understanding. In Proceedings of the IEEE/CVF Conference on Computer Vision and Pattern Recognition Workshops (pp. 0-0).
11. Zhang, Z., Yu, S., Yang, S., Zhou, Y., & Zhao, B. (2021). Rail-5k: A real-world dataset for rail surface defects detection. ArXiv preprint arXiv: 2106.14366.